

<https://doi.org/10.1038/s41612-024-00713-2>

Tropical eastern Pacific cooling trend reinforced by human activity

Check for updates

Eui-Seok Chung¹, Seong-Joong Kim²✉, Sang-Ki Lee³, Kyung-Ja Ha^{4,5,6}, Sang-Wook Yeh⁷, Yong Sun Kim^{8,9}, Sang-Yoon Jun¹, Joo-Hong Kim¹ & Dongmin Kim^{3,10}

It remains unresolved whether the La Niña-like sea surface temperature (SST) trend pattern during the satellite era, featuring a distinct warming in the northwest/southwest Pacific but cooling in the tropical eastern Pacific, is driven by either external forcing or internal variability. Here, by conducting a comprehensive analysis of observations and a series of climate model simulations for the historical period, we show that a combination of internal variability and human activity may have shaped the observed La Niña-like SST trend pattern. As in observations, SSTs in each model ensemble member show a distinct multi-decadal swing between El Niño-like and La Niña-like trend patterns due to internal variability. The ensemble-mean trends for some models are, however, found to exhibit an enhanced zonal SST gradient along the equatorial Pacific over periods such as 1979–2010, suggesting a role of external forcing. In line with this hypothesis, single-forcing large ensemble model simulations show that human-induced stratospheric ozone depletion and/or aerosol changes have acted to enhance the zonal SST gradient via strengthening of Pacific trade winds, although the effect is model dependent. Our finding suggests that the La Niña-like SST trend is unlikely to persist under sustained global warming because both the ozone and aerosol impacts will eventually weaken.

Changes in the spatial distribution of SST in the tropical Pacific in response to increasing concentrations of greenhouse gases have substantial implications for the global climate^{1–4}. Yet, unlike observations that exhibit a La Niña-like SST trend pattern since the late 1970s^{5–7}, characterized by enhanced warming in the northwest and southwest Pacific but cooling in the tropical eastern Pacific (e.g., Fig. 1b), climate models under the historical forcing scenario rarely reproduce such a spatial pattern^{3,4,8–11}, undermining the confidence in model-projected human-induced climate changes.

Considering that El Niño-Southern Oscillation (ENSO) is the major predictability source and scientific basis for short-term climate predictions, attributing the causes for the tropical mean state change is essential for understanding its impact on ENSO and resulting change in ENSO characteristics. For instance, with the strengthened zonal SST gradient across the tropical Pacific and the westward shift of the dominant region of the atmosphere-ocean coupling associated with ENSO since 1999/2000, ENSO has shifted to a smaller variability and higher frequency regime^{12–14}; the

related breakdown of the connection between ENSO SST and warm water volume^{14,15} caused a degradation of ENSO prediction skills^{12,16}. A recent study¹⁷ also documented the key role of the tropical Pacific mean state changes in the evolution and prediction of the triple-dip La Niña in 2020–2023.

A variety of hypotheses have been proposed to explain the observed tropical eastern Pacific cooling trend amid ongoing increases in greenhouse gas concentrations, including an ocean dynamic thermostat mechanism^{18,19}, rectification of the mean state due to weakening non-linear ENSO amplitude²⁰, inter-basin teleconnections^{8,21–25}, spatially inhomogeneous aerosol forcing^{19,26–29}, Southern Ocean cooling^{30,31} due to Antarctic melt-water discharge³ and/or strengthened westerlies over the Southern Ocean, and internal variability^{10,32–37}. However, there is still a lack of consensus on the origin of the observed tropical eastern Pacific cooling trend^{3,4,11,35,37–40}. It also remains inconclusive whether the cooling trend will persist under sustained global warming.

¹Division of Ocean and Atmosphere Sciences, Korea Polar Research Institute, Incheon, South Korea. ²Office of Vice President, Korea Polar Research Institute, Incheon, South Korea. ³Atlantic Oceanographic and Meteorological Laboratory, NOAA, Miami, FL, USA. ⁴Center for Climate Physics, Institute for Basic Science, Busan, South Korea. ⁵Department of Climate System, Pusan National University, Busan, South Korea. ⁶BK21 School of Earth and Environmental Systems, Pusan National University, Busan, South Korea. ⁷Department of Marine Sciences and Convergent Technology, Hanyang University, Ansan, South Korea. ⁸Ocean Circulation and Climate Research Department, Korea Institute of Ocean Science and Technology, Busan, South Korea. ⁹Ocean Science, University of Science and Technology, Daejeon, South Korea. ¹⁰Cooperative Institute for Marine and Atmospheric Studies, University of Miami, Miami, FL, USA.

✉ e-mail: seongkim@kopri.re.kr

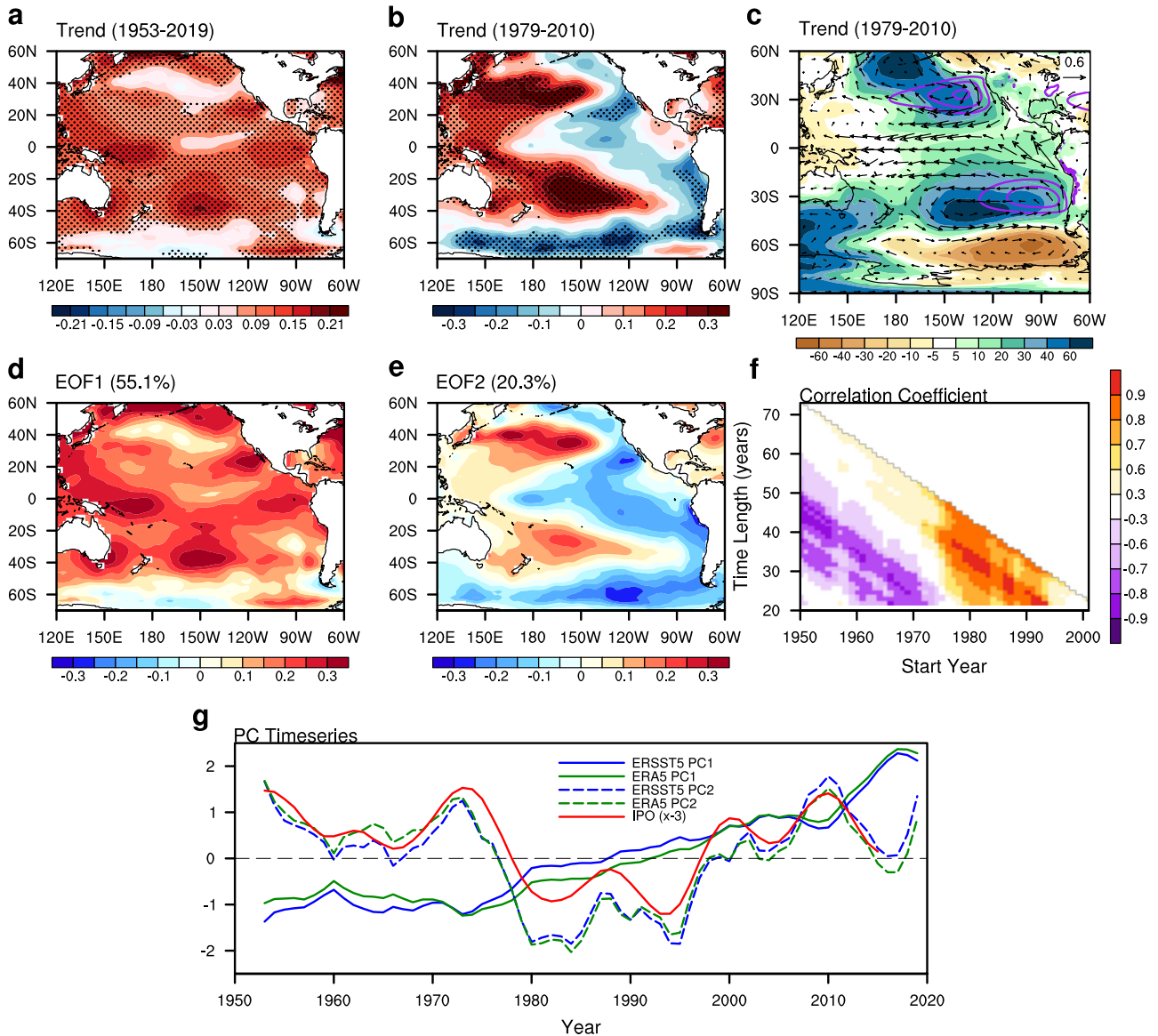


Fig. 1 | Characteristics of the observed change and variability over the Pacific. **a** SST trends over the period 1953–2019 from ERSST5, with stippling indicating statistical significance of the computed trends at the 95% confidence level. **b** Same as in **a**, but over the period 1979–2010. **c** Sea level pressure (shading) and 850-hPa wind (vectors) trends over the period 1979–2010 from ERA5. Contours in purple represent the climatological high-pressure regions. **d** Spatial pattern of the first EOF mode analyzed in the Pacific (70°S–60°N, 120°E–60°W) over the period 1953–2019 for 7-yr running-mean, annual-mean SST anomaly. **e** Same as in **d**, but for the

second EOF mode. **f** Spatial pattern correlation over the Pacific between the second EOF mode shown in **e** and observed SST trends over multiple periods. In **f**, x-axis denotes the start year of a given period with y-axis representing the time span. **g** Time series of the standardized PC values corresponding to the first two leading EOF modes shown in **d** and **e**. Also shown are the PC time series computed with ERA5 SST (lines in green) and the observed time series of low-pass filtered IPO index multiplied by -3 (red line).

Recently, the onset of the Antarctic ozone hole has been proposed as a driver of the tropical eastern Pacific cooling trend⁹. This is because resultant increases in meridional temperature gradients may lead to a Southern Ocean cooling via a strengthening of the Southern Hemispheric westerlies; this cooling could subsequently propagate into the tropical Pacific by atmospheric eddies, equatorward Ekman transport, and climatological southeasterlies along the west coast of South America^{9,30,31}. The cooling in the tropical eastern Pacific may then be amplified by wind-evaporation-SST feedback, cloud feedback, and coastal upwelling, along with Bjerknes feedback^{9,30,31}. However, the stratospheric ozone depletion appears to have paused after around 2000 as a result of the Montreal Protocol^{41,42}, suggesting that stratospheric ozone depletion alone may not explain the whole picture. Moreover, prior work showed that even if the observed Southern Ocean cooling trends, that might have resulted from stratospheric ozone depletion,

are nudged in coupled model simulations, the cooling does not penetrate deep enough to the equatorial Pacific⁴³. This implies that multiple forcing agents and/or internal variability are involved in driving the tropical eastern Pacific cooling trend. In fact, the contrasting multi-decadal SST trends between the northwest/southwest Pacific and the tropical eastern Pacific might occur due to low-frequency internal climate variability^{10,32–37}, in particular the Inter-decadal Pacific Oscillation (IPO) or Pacific Decadal Oscillation (PDO). Consistent with this hypothesis, despite model biases and errors^{3,4,8,10,11,35,40,44–46}, previous studies showed that many aspects of the observed multi-decadal changes could be explained, in part, by internal variability^{10,32–37,47–51}.

In this study, by analyzing a series of climate model simulations along with observations over a period including the pre-satellite era, we investigate the roles of external forcings and internal variability in driving the

contrasting SST trend pattern between the northwest/southwest Pacific and the tropical eastern Pacific. We begin by analyzing the characteristics of observed Pacific SST change and variability over an extended period, and then explore the impact of the IPO on the tropical eastern Pacific cooling trends over the satellite era. Finally, single-forcing large ensemble simulations are analyzed to determine the role of external forcing agents in driving a cooling trend over the tropical eastern Pacific.

Results

Observed SST and atmospheric circulation changes in the Pacific

Before tackling the primary causes for the tropical eastern Pacific cooling trend during the satellite era, we examine the overall characteristics of the observed Pacific SST change and variability (Methods). The observed SST trends over the period 1953–2019 indicate spatial inhomogeneity in warming, including muted and insignificant warming in the central equatorial Pacific and extratropical North Pacific (Fig. 1a). However, the previously reported La Niña-like SST trend pattern during the satellite era (e.g., Fig. 1b) is absent. An empirical orthogonal function (EOF) analysis is conducted to identify the leading modes of variability using the 7-year running-mean, annual-mean SST anomalies in the Pacific (70°S–60°N, 120°E–60°W) over the same period (Methods). The leading EOF mode, which explains 55.1% of the total variance, is far from a La Niña-like pattern (Fig. 1d); the corresponding principal component (PC) of the leading mode shows an overall steady increase over time (solid lines in Fig. 1g). In contrast, the La Niña-like pattern appears as the second EOF mode, explaining 20.3% of the total variance (Fig. 1e). The corresponding PC time series exhibit multi-decadal fluctuations (dashed lines in Fig. 1g) including a positive trend over 1980–2010, suggesting that the second EOF mode is closely linked to multi-decadal internal variability. In line with this hypothesis, the temporal evolution of PC2 is highly correlated with a low-pass filtered IPO index⁵², which is characterized by a positive-to-negative phase shift during the satellite era.

SST trends are also computed for other periods to determine whether the observed spatial patterns might vary substantially due to internal variability (Methods). Spatial pattern correlations over the Pacific between SST trends and the second EOF mode shown in Fig. 1e indicate that a La Niña-like SST trend pattern has not always been observed over the past 70 years (Fig. 1f). Specifically, while recent periods starting from the late 1970s show positive correlations with the largest value observed over 1982–2014, earlier periods (e.g., 1950–1994) tend to show negative correlations (i.e., El Niño-like SST trend pattern). Indeed, a marked contrast is evident between 1950–1994 (Supplementary Fig. 1d–f; El Niño-like pattern and a weakening of atmospheric circulation) and 1982–2014 (Supplementary Fig. 1a–c; La Niña-like pattern along with strengthened circulation), highlighting multi-decadal variability in the Pacific.

Given that both the PC2 and IPO time series exhibit a large change over the period of 1979–2010 with a high co-variability (Fig. 1g), we next examine the observed SST and related atmospheric circulation trends focusing on that period. As noted in previous studies^{3,5–9,11,24,46,51}, observations indicate a cooling trend in the tropical eastern Pacific (Fig. 1b and Supplementary Fig. 2a, b), contrasting a pronounced warming trend in the northwest and southwest Pacific. This SST trend pattern is accompanied by a distinct cooling trend in the Southern Ocean, which has been attributed in part to internal variability associated with both tropical teleconnection^{51,53–56} and local factors⁵⁷ including the Southern Annular Mode. On the other hand, a forced SST response inferred from model simulations integrated with observed time-varying external forcings (Methods) fails to reproduce the distinct cooling trends (Supplementary Fig. 2c–i). This model-observation discrepancy could be attributed to model biases and deficiencies^{3,4,8,10,11,35,40,46}. However, for some models such as the CESM2 LE and IPSL-CM6A-LR, the ensemble-mean changes exhibit an enhanced zonal SST gradient across the equatorial Pacific (Supplementary Fig. 2c, d and Supplementary Fig. 3), suggesting the role of external forcing in driving a cooling trend over the tropical eastern Pacific. Concurrent changes in sea level pressure and 850-

hPa winds over the tropical Pacific estimated from a reanalysis dataset (Methods) suggest a strengthening of the Pacific Walker circulation^{11,21,25,34,50} (Fig. 1c). The accompanying intensification of the Pacific trade winds, which are also related to a strengthening of both the Hadley¹¹ and Southern Hemisphere Ferrel⁵⁸ cells, are expected to induce tropical eastern Pacific cooling^{11,21,25,50}.

Impact of internal variability on the tropical eastern Pacific cooling trend

Based on the potential linkage between the La Niña-like SST trend pattern and the IPO (Fig. 1), we first examine the role of internal variability by conducting an EOF analysis for annual-mean SST trends over 1979–2010 across 50 ensemble members of the CESM2 LE⁵⁹ (Methods). The spatial pattern of the leading inter-ensemble EOF mode of variability appears to be related to the IPO (Fig. 2b), with a large inter-ensemble spread (Fig. 2c). Two sets of SST trends are computed, one using the ensemble members with their PC values at the top 10%, and the other at the bottom 10%. Similarly, the composite mean trends for sea level pressure and 850-hPa winds are computed for the two subsets. Although these ensemble members were integrated with the same external forcing, the resulting SST and circulation trend patterns dramatically differ between the two groups (Fig. 2d–i). They are also distinguished from the ensemble-mean SST trends (Fig. 2a). The top 10% subset qualitatively reproduces the observed changes of the recent period; therefore, it appears that internal variability plays an important role in driving a cooling trend over the tropical eastern Pacific.

To further explore and quantify the role of internal variability, the CESM2 LE ensemble-mean SST anomalies are subtracted from ERSST5 SST anomalies since both external forcing agents and internal variability may affect the observed SSTs. An EOF analysis is then conducted over the Pacific for the period 1953–2019, assuming that the difference largely represents internal variability. The leading EOF mode shows a spatial pattern characterized by opposite signs between the northwest/southwest Pacific and the tropical eastern Pacific (Supplementary Fig. 4a); the corresponding PC time series is closely related to the IPO including a comparable temporal evolution over 1980–2010, with other models showing a similar feature (Supplementary Fig. 4c). Note that a similar spatial pattern appears as the leading EOF mode from pre-industrial control simulation (Supplementary Fig. 4b). The atmospheric circulation patterns derived from the ERSST5 minus model ensemble mean are also qualitatively comparable with those derived from the pre-industrial control simulation (Supplementary Figs. 4d, e), further supporting a definite role of internal variability in producing the observed cooling trend in the tropical eastern Pacific.

The clear role of the IPO in both observations and large ensemble model simulations might lead one to conclude that the tropical eastern Pacific cooling trend over the satellite era could be attributed almost entirely to internal climate variability. However, prior work indicated that a small fraction of model simulations can match the observed strengthening of the Pacific trade winds²⁶, although it cannot be ruled out that climate models might have deficiencies in representing internal climate variability⁴⁴ as well as the forced response^{10,40}. Moreover, the ensemble-mean SST trends exhibit a strengthened zonal SST gradient along the equatorial Pacific in some climate models, such as the CESM2 LE and IPSL-CM6A-LR, when forced by external forcing agents (Supplementary Figs. 2c, d and Supplementary Fig. 3). It is also noted that as in these two models, a slight cooling or muted warming trend is produced over the southeast Pacific centered around 30°S in other models. These model results suggest a possibility that both internal variability and certain external forcing agents have acted in the same direction to drive the tropical eastern Pacific cooling trend and related circulation changes over the satellite era.

Linkages of the tropical eastern Pacific cooling trend to external forcings

In this section, CMIP6 single-forcing simulations for IPSL-CM6A-LR and HadGEM3-GC31-LL along with the CESM2 Single Forcing Large Ensemble Project⁶⁰ are analyzed in conjunction with all-forcing simulations

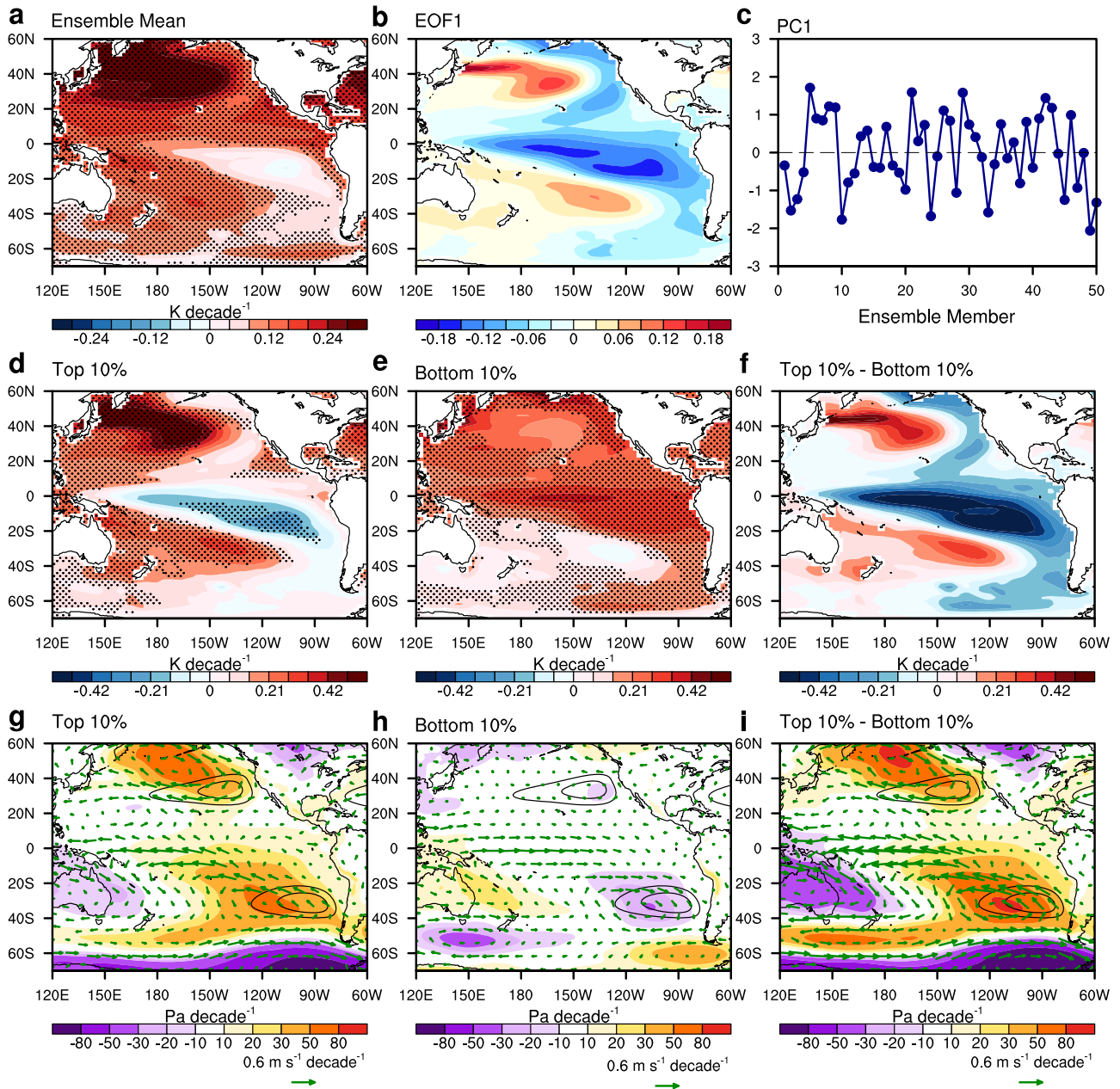


Fig. 2 | Inter-ensemble variability of simulated SST trends due to internal climate variability. **a** Ensemble-mean of annual-mean SST trends over the period 1979–2010 for the CESM2 LE with stippling denoting regions where more than 70% of the ensemble members exhibit the same sign. **b** Spatial pattern of the first EOF mode for the 1979–2010 SST trends across the ensemble members. **c** Corresponding standardized PC. **d** Spatial pattern of SST trends averaged over the ensemble

members with their PC values at the top 10%. Stippling indicates regions where the corresponding ensemble members exhibit the same sign. **e** Same as in **d**, but for the ensemble members with their PC values at the bottom 10%. **f** Difference in the mean SST trends between the top 10% and bottom 10% subsets. **g–i** Same as in **d–f**, but for trends in sea level pressure (shading) and 850-hPa winds (vectors) with contours in black denoting the climatological high-pressure regions.

(the CESM2 LE for the CESM2 Single Forcing Large Ensemble Project) to investigate the role of external forcings (specifically, changes in greenhouse gas concentrations, anthropogenic aerosols, and stratospheric ozone concentrations) in the tropical eastern Pacific cooling trend and related atmospheric circulation changes (Methods). We particularly focus on IPSL-CM6A-LR for two reasons: 1) the ensemble-mean SST trends indicate a strengthened zonal SST gradient along the equatorial Pacific as in observations and 2) the CMIP6 archive provides model simulation output for the hist-stratO3 experiment in which external forcing agents were fixed at their preindustrial levels except for stratospheric ozone concentrations⁶¹.

In IPSL-CM6A-LR, HadGEM3-GC31-LL and the CESM2 Single Forcing Large Ensemble Project, an increase in greenhouse gas concentrations over various periods of the satellite era tends to induce a strengthening

of westerlies over the Southern Ocean^{62,63} (Supplementary Fig. 5a–c). This may result in a surface cooling in the southeastern Pacific by atmospheric eddies, equatorward Ekman transport, and climatological southeasterlies^{9,30,31}; the resulting cooling might in turn propagate into the equatorial Pacific via interplay between SST, low-level clouds and atmospheric/oceanic circulations^{9,30,31}, leading to a cooling trend over the tropical eastern Pacific. Accompanying sea level pressure and 850-hPa wind changes over the equatorial Pacific, however, suggest a weakening of the Pacific Walker circulation (Supplementary Fig. 5a–c), thereby resulting in a decrease, rather than increase, in zonal SST gradient along the equatorial Pacific (Supplementary Fig. 6a–c). In line with previous studies suggesting the role of aerosol changes^{19,26,29}, the CESM2 Single Forcing Large Ensemble Project simulations produce an enhanced cooling trend over the tropical

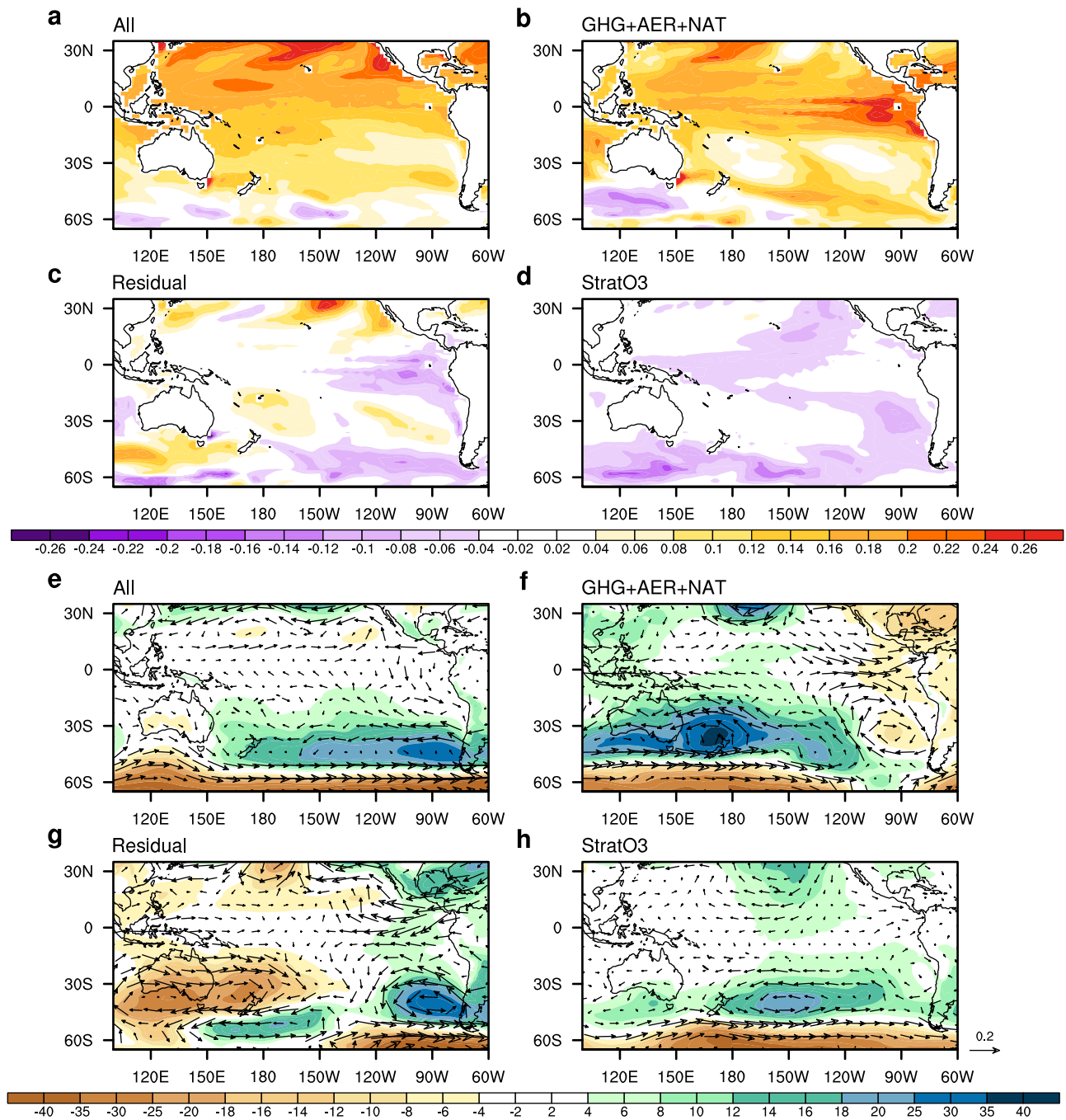


Fig. 3 | Impact of stratospheric ozone forcing on SST and atmospheric circulation over the Pacific. **a** Ensemble-mean SST trends (unit: K decade⁻¹) over 1979–2010 for IPSL-CM6A-LR in response to all forcing agents. **b** Same as in **a**, but for the sum of SST trends for the corresponding greenhouse gas-only (GHG), anthropogenic aerosol-only (AER) and natural forcing-only (NAT) experiments. **c** Difference between **a** and **b**. **d** Same as in **a**, but for the corresponding stratospheric ozone-only (StratO3) experiment. **e–h** Same as in **a–d**, but for trends in sea level pressure (shading, unit: Pa decade⁻¹) and 850-hPa winds (vectors, unit: m s⁻¹ decade⁻¹).

eastern Pacific and the Pacific sector of the Southern Ocean in response to imposed anthropogenic aerosol forcing (Supplementary Fig. 6e), which is accompanied by a strengthening of the Pacific trade winds and enhanced east-west contrast in sea level pressure over the tropical Pacific, especially from 1979 to the early 2000s (Supplementary Fig. 5e). The spatial pattern of the aerosol forcing-induced SST trends, however, appears to be sensitive to a given time period (Supplementary Fig. 6e); in addition, the impacts of anthropogenic aerosol forcing on SST and atmospheric circulation over the Pacific are virtually negligible for HadGEM3-GC31-LL (Supplementary Figs. 5f and 6f). Moreover, the IPSL-CM6A-LR produces a greater cooling over the equatorial western Pacific than over the east in response to the imposed anthropogenic aerosol forcing (Supplementary Fig. 6d). These

discrepancies indicate a substantial model dependency of the linkage between anthropogenic aerosol forcing and the tropical eastern Pacific cooling trend.

In IPSL-CM6A-LR, unlike for the greenhouse gas-only and anthropogenic aerosol-only simulations (Supplementary Figs. 6a, d), the corresponding all-forcing experiment produces a strengthened zonal SST gradient along the equatorial Pacific (Fig. 3a and Supplementary Fig. 7a), which is accompanied by anomalous anticyclonic circulation over the southeastern Pacific and related strengthening of the Pacific trade winds (Fig. 3e and Supplementary Fig. 8a). These discrepancies might result from natural forcing (i.e., changes in volcanic eruptions and solar activity); however, the sum of the trends for the greenhouse gas-only, anthropogenic

aerosol-only and natural forcing-only simulations (Fig. 3b, f and Supplementary Figs. 7b and 8b) cannot fully explain the SST and circulation trends for the all-forcing experiment (Fig. 3a, e and Supplementary Figs. 7a and 8a). Similar discrepancies also exist between the CESM2 LE (Fig. 2a) and the corresponding single forcing simulations (Supplementary Fig. 6b, e) for the period 1979–2010. These results therefore suggest the role of other non-greenhouse gas forcing agents in driving a cooling trend over the tropical eastern Pacific and associated circulation changes.

The differences in SST trend between the all forcing experiment and the sum of greenhouse gas-only, anthropogenic aerosol-only and natural forcing-only experiments for IPSL-CM6A-LR exhibit a strengthened zonal SST gradient along the equatorial Pacific accompanied by pronounced cooling in the Pacific sector of the Southern Ocean (Fig. 3c and Supplementary Fig. 7c). The corresponding differences in sea level pressure and 850-hPa wind trends also suggest a strengthening of the Pacific Walker circulation (Fig. 3g and Supplementary Fig. 8c). Unlike in the greenhouse gas-only and anthropogenic aerosol-only experiments, the sea level pressure and 850-hPa wind trends for the stratospheric ozone-only experiment indicate an enhanced zonal pressure gradient over the tropical Pacific as well as anomalous anticyclonic circulation over the southeastern Pacific (Fig. 3h and Supplementary Fig. 8d), which are conducive to driving a cooling trend over the tropical eastern Pacific (Fig. 3d and Supplementary Fig. 7d) via a strengthening of the Pacific trade winds. Despite the noticeable impact of stratospheric ozone depletion, the eastern tropical Pacific cooling patterns are different between Fig. 3c, d (also between Supplementary Fig. 7c and Supplementary Fig. 7d): the residual shows the cooling near the equator but the ozone-induced response accompanies cooling in the subtropical regions. This difference might be linked to non-linear interactions between stratospheric ozone depletion and greenhouse gas forcing and/or other forcing agents as well as model biases and dependency. The residual changes shown in Fig. 3c and Supplementary Fig. 7c might also be attributed to changes in land use and/or biomass burning emissions. However, the multi-model, multi-ensemble-mean SST trends resulting from the land-use change (Supplementary Fig. 9e), estimated by subtracting the CMIP6 hist-noLu⁶⁴ from the corresponding historical experiment, are unlikely to fully explain the residual SST trends; in addition, the CESM2 Single Forcing Large Ensemble Project biomass burning emission experiment produces a weak warming trend over the southeastern Pacific and the Pacific sector of the Southern Ocean (Supplementary Fig. 9f).

The CESM2 Single Forcing Large Ensemble Project everything else (EE) experiment includes the influences of natural forcing agents and land-use change, but the resulting trends in SST and atmospheric circulation (Fig. 4a, e and Supplementary Figs. 10a and 11a) are qualitatively consistent with those for the IPSL-CM6A-LR stratospheric ozone-only experiment. Similar results are also obtained from the HadGEM3-GC31-LL total (tropospheric plus stratospheric) ozone-only experiment (Fig. 4c, g and Supplementary Figs. 10c and 11c). Although changes in tropospheric ozone concentration are likely to induce an overall warming trend⁶⁵, the SST and atmospheric circulation trends for the total ozone-only experiment are in line with the residual trends computed by subtracting the sum of greenhouse gas-only, anthropogenic aerosol-only and natural forcing-only experiments from the corresponding all-forcing run (Fig. 4b, f and Supplementary Figs. 10b and 11b). The multi-model, multi-ensemble-mean differences between the historical and hist-1950HC (in which ozone-depleting substances were fixed at their 1950 levels⁶⁶) experiments, which represent the impact of time-varying ozone-depleting substances and resulting stratospheric ozone concentration changes, also exhibit a pronounced strengthening of westerlies over the Southern Ocean and anticyclonic circulation in the southeastern Pacific (Fig. 4h and Supplementary Fig. 11d), thereby playing a role in inducing a cooling trend over the tropical eastern Pacific (Fig. 4d and Supplementary Fig. 10d). In addition, southerly wind anomalies found over the Southeast Pacific adjacent to the west coast of South America (Fig. 4h and Supplementary Fig. 11d) are likely to contribute to eastern Pacific cooling via both coastal upwelling³⁰ and equatorward advection^{3,9,30,31,67}. Previous studies showed that stratospheric ozone depletion-induced cooling

has acted to intensify the eddy-driven jet^{58,68,69} and an overall poleward shift and strengthening of the Southern Hemispheric Ferrel cell⁵⁸. Hence, although ozone-depleting substances are powerful greenhouse gases^{70–73}, stratospheric ozone depletion in Antarctica and its feedback/interactions with other forcing agents might induce cooling in the tropical eastern Pacific through intensified Pacific trade winds.

In contrast to the distinct impact of the stratospheric ozone depletion evident in IPSL-CM6A-LR, the stratospheric ozone-only experiment for CanESM5 and MIROC6 produces indistinct SST changes or inconsistent features with the residual fields (Supplementary Fig. 9a–d). As in the case for anthropogenic aerosols, these inter-model discrepancies seem to indicate a model dependency in the linkage between stratospheric ozone depletion and the tropical eastern Pacific cooling trend.

Finally, to quantify the impact of forcing agents on the trends in the tropical Pacific zonal SST gradient and the Pacific Walker circulation, we computed the ensemble-mean trends in the SST difference between the western Pacific (10°S–10°N, 110°E–180°) and the eastern Pacific (10°S–10°N, 180°–80°W) and the sea level pressure difference between the eastern Pacific (5°S–5°N, 160°W–80°W) and the western Pacific (5°S–5°N, 80°E–160°E)⁷⁴ over various periods for single-forcing large ensemble simulations. Figure 5 indicates that the zonal SST gradient and the Pacific Walker circulation tend to weaken in response to greenhouse gas forcing and biomass burning emissions in model simulations. In contrast, stratospheric ozone-only (for IPSL-CM6A-LR), total ozone-only (for HadGEM3-GC31-LL), EE (for CESM2 Single Forcing Large Ensemble Project), and historical minus hist-1950HC (for multiple models) simulations, represented by stars, exhibit an overall strengthening. A similar strengthening results from changes in anthropogenic aerosols and land use; however, large differences between models and between analysis periods appear to indicate that their impacts are relatively less robust relative to that of ozone depletion in model simulations.

Discussion

In this study, we analyzed various climate model simulations along with observations to address the contrasting SST trends between the northwest/southwest Pacific and the tropical eastern Pacific over the satellite era after 1979. The tropical Pacific SST is found to have undergone substantial multi-decadal fluctuations over the past 70 years, principally due to internal climate variability associated with the IPO, leading to the tropical eastern Pacific cooling trend during the satellite era. However, the enhanced zonal SST gradient along the equatorial Pacific is qualitatively captured by some realizations of large-ensemble climate model simulations driven by observed external forcing. Therefore, we further analyzed single-forcing large ensemble model simulations to determine if there are any specific external forcing agents acting to produce a cooling trend over the tropical eastern Pacific. While climate model simulations integrated with increasing concentrations of greenhouse gases tend to exhibit an El Niño-like SST trend pattern associated with weakened easterly winds over the tropical Pacific, model simulations forced by non-greenhouse gas forcing agents produce a cooling trend over the tropical eastern Pacific via strengthened Pacific trade winds associated with enhanced anticyclonic circulations over the subtropical South Pacific. In particular, as suggested in previous studies^{9,19,26–29}, stratospheric ozone depletion and anthropogenic aerosols are found to play an important role, albeit with a substantial inter-model discrepancy. Therefore, we conclude that both internal variability and non-greenhouse gas forcing have acted in the same direction to shape the tropical eastern Pacific cooling trend over the satellite era.

Despite the enhanced zonal SST gradient along the equatorial Pacific in single-forcing large ensemble model simulations integrated with non-greenhouse gas forcing agents, all-forcing model simulations rarely capture the observed cooling trends over the tropical eastern Pacific as well as over the Southern Ocean. Such failures can be caused by model biases and/or deficiencies^{10,40}, including distinctly weaker stratocumulus cloud feedback over the southeastern tropical Pacific³⁰. It is also possible that climate models might overestimate greenhouse gas forcing-induced warming while underestimating non-greenhouse gas forcing-induced cooling over the

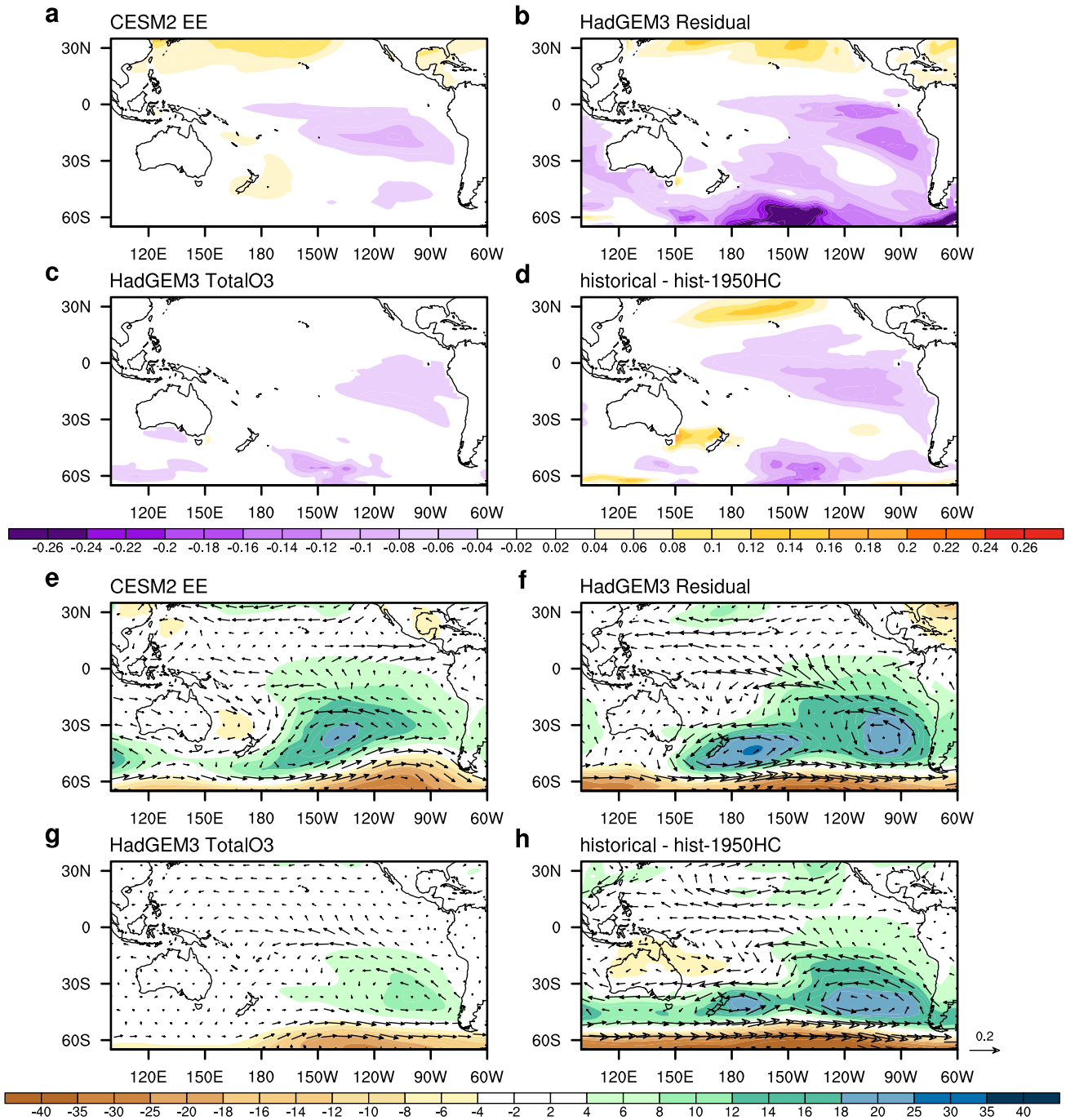


Fig. 4 | Potential role of the stratospheric ozone depletion in a cooling trend over the tropical eastern Pacific. **a** Ensemble-mean SST trends (unit: K decade^{-1}) over 1979–2010 for the CESM2 Single Forcing Large Ensemble Project EE (everything else except for greenhouse gases, anthropogenic aerosols and biomass burning emissions) experiment. **b** Similar to **a**, but for the SST trend difference between the all-forcing experiment and the sum of the corresponding greenhouse gas-only, anthropogenic aerosol-only and natural forcing-only simulations for HadGEM3-

GC31-LL. **c** Same as in **a**, but for the HadGEM3-GC31-LL total (tropospheric plus stratospheric) ozone forcing-only experiment. **d** Similar to **a**, but for the multi-model, multi-ensemble SST trend difference between the historical and hist-1950HC simulations, which represents the impact of time-varying ozone depleting substances and resultant stratospheric ozone concentration changes. **e–h** Same as in **a–d**, but for trends in sea level pressure (shading, unit: Pa decade^{-1}) and 850-hPa winds (vectors, unit: $\text{m s}^{-1} \text{decade}^{-1}$).

tropical Pacific and the Southern Ocean, and/or underestimate multi-decadal internal variability⁴⁴. Given that the observational record is regarded as one realization, effectively devising a coordinated multi-model, multi-ensemble experimental design is needed to resolve the model-observation discrepancy. In addition to possible biases in the externally forced response, the model-observation discrepancy might also result from the model deficiency in reproducing the ENSO SST pattern in the tropical Pacific and ENSO frequency⁷⁵.

Some studies suggest that the stratospheric ozone depletion is unlikely the main factor leading to a surface cooling of the Southern Ocean^{42,76}. This implies that the Southern Ocean cooling may not be the main pathway by which the stratospheric ozone depletion leads to the tropical eastern Pacific cooling trend. However, considering large thermal inertia of the Southern Ocean, SST anomalies resulting from the Southern Annular Mode (SAM) may feed back to the atmosphere and thus modulate the persistence of the SAM⁷⁷. Although it is unclear

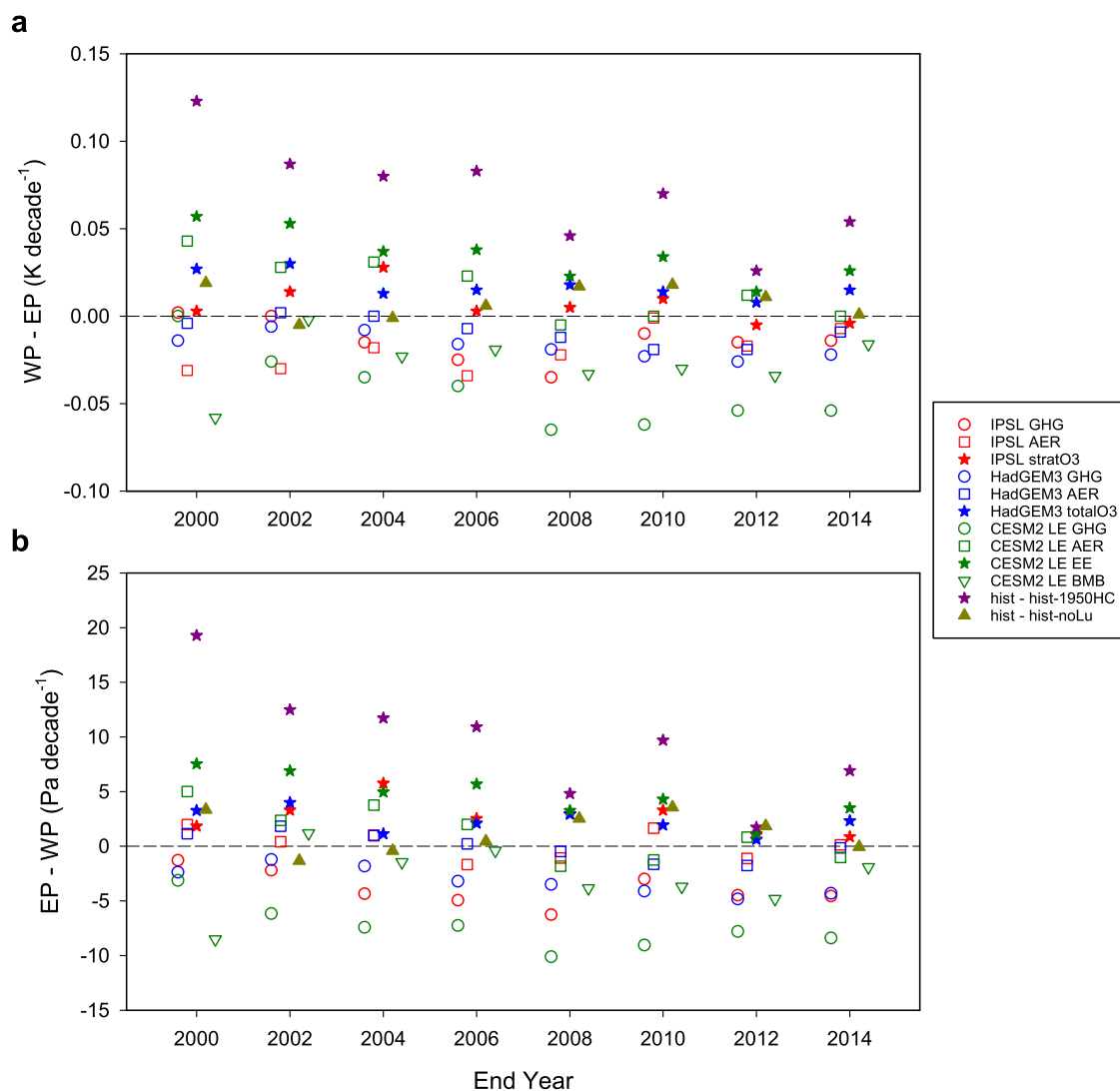


Fig. 5 | Impact of external forcing agents on the tropical Pacific zonal SST gradient and the Pacific Walker circulation. **a** Ensemble-mean trends in the zonal SST gradient, defined as the SST difference between the western Pacific (10°S–10°N, 110°E–180°) and the eastern Pacific (10°S–10°N, 180°–80°W), under greenhouse gas-only (GHG, open circles), anthropogenic aerosol-only (AER, open squares), stratospheric ozone-only (filled stars in red), total ozone-only (filled stars in blue), and biomass burning emission-only (BMB, inverted open triangle in green) scenarios for IPSL-CM6A-LR, HadGEM3-GC31-LL, and the CESM2 Single Forcing Large

Ensemble Project. Also shown are the ensemble-mean trends for the CESM2 Single Forcing Large Ensemble Project EE (filled stars in green) experiment and the multi-model, multi-ensemble mean trends for the historical minus hist-1950HC (filled stars in purple) and the historical minus hist-noLu (filled triangle in dark yellow) experiments. The x-axis denotes the end year of a given period starting from 1979. **b**, Same as in **a**, but for the difference in sea level pressure between the eastern Pacific (5°S–5°N, 160°W–80°W) and the western Pacific (5°S–5°N, 80°E–160°E).

whether the Southern Ocean cooling is involved, our analysis clearly shows that the stratospheric ozone depletion can induce the tropical eastern Pacific cooling trend via a strengthening of the Pacific trade winds.

An important outstanding question is whether the current tropical eastern Pacific cooling trend will persist and/or intensify in the future. Although other factors such as Antarctic meltwater discharge³ and resulting Southern Ocean cooling^{30,31} have also played a role, projected Antarctic ozone recovery^{41,42,60} and reductions in anthropogenic aerosol emissions over Asian regions might lead to a warming trend^{78,79} in the future if other conditions remain the same. Thus, on the premise that the model-simulated response to greenhouse gas forcing is largely consistent with reality in spite of model deficiency in representing ocean stratification²⁰, the near-future pathways of non-greenhouse gas forcing may have critical implications for the global climate and the climate sensitivity^{2,59,80,81}.

Methods

Observational datasets

We examined observed SST changes using NOAA’s Extended Reconstructed Sea Surface Temperature version 5 (ERSST5)⁸² for 1950–2022 along with the European Centre for Medium-Range Weather Forecasts Reanalysis version 5 (ERA5) dataset⁸³, although these interpolated datasets might disagree with quality-checked, bias-adjusted non-interpolated datasets in the tropical Pacific³⁸, especially, over the central-to-eastern Pacific, due to insufficient spatiotemporal sampling of in situ measurements. Note that the Hadley Centre Sea Ice and Sea Surface Temperature (HadISST) SST dataset⁸⁴ exhibits similar trends to ERSST5 and ERA5 (Fig. 1b and Supplementary Fig. 2a, b). Due to the lack of long-term observations, despite potential uncertainties and errors in atmospheric circulation trends estimated from reanalysis products⁸⁵, the ERA5 reanalysis dataset is also used as a proxy for observations to examine changes in sea level pressure, zonal and meridional winds, and meridional overturning circulation. We also used a

low-pass filtered Inter-decadal Pacific Oscillation (IPO) index⁵² (<https://psl.noaa.gov/data/timeseries/IPOTPI/>) as a proxy for internal climate variability over the Pacific on multi-decadal timescales, which is defined as the SST anomaly averaged over the central equatorial Pacific (10°S–10°N, 170°E–90°W) minus the average of the SST anomaly in the northwest Pacific (25°N–45°N, 140°E–145°W) and southwest Pacific (50°S–15°S, 150°E–160°W).

Model simulation output

The observed changes in SST and atmospheric variables are compared with model simulations conducted as part of the Coupled Model Inter-comparison Project phase 6 (CMIP6)⁸⁶ as well as the Community Earth System Model version 2 (CESM2) Large Ensemble (CESM2 LE) simulations⁵⁹, both of which were integrated with the CMIP6 historical forcing (i.e., observed time-varying external forcing agents) over the period 1850–2014. As the CMIP6 historical forcing experiment does not cover the most recent period 2015–2022, the historical forcing scenario is concatenated with a projected future forcing scenario of CMIP6 (i.e., Shared Socioeconomic Pathway (SSP) forcing scenario SSP3-7.0 or SSP2-4.5). For the CESM2 LE, we only used a 50-member subset integrated with a smoothed version of biomass burning dataset over 1990–2020 to avoid artificial discontinuities in biomass burning emissions⁵⁹. Meanwhile, given that the externally forced response can be obscured by internal climate variability, the model-simulated forced response is estimated only for a subset of the CMIP6 models that provide simulation output for more than 25 ensemble members over the period 1979–2010: IPSL-CM6A-LR (33 ensemble members), HadGEM3-GC31-LL (50 ensemble members), MIROC6 (50 ensemble members), CanESM5 (50 ensemble members), MPI-ESM1-2-LR (30 ensemble members), and ACCESS-ESM1-5 (40 ensemble members), along with the CESM2 Large Ensemble (50 ensemble members).

To determine the role of external forcing agents in driving the tropical eastern Pacific cooling trend, the CMIP6 single-forcing simulations, consisting of greenhouse gas-only (hist-GHG⁶¹), anthropogenic aerosol-only (hist-aer⁶¹), natural forcing (volcanic eruptions and solar activity)-only (hist-nat⁶¹), stratospheric ozone-only (hist-stratO3⁶¹) and total (tropospheric plus stratospheric) ozone-only (hist-totalO3), are analyzed in conjunction with the corresponding all-forcing simulations. For a given model, residual trends are computed to roughly estimate the combined impact of land-use change, biomass burning emissions and stratospheric ozone depletion by subtracting the sum of the hist-GHG, hist-aer and hist-nat from the corresponding all-forcing experiment for all ensemble members for which simulation output is available for these four experiments. We also used the CESM2 Single Forcing Large Ensemble Project⁶⁰ output in conjunction with the CESM2 LE. The CESM2 Single Forcing Large Ensemble Project consists of a series of coupled model simulations integrated with individual forcing agents, i.e., time-varying greenhouse gas concentrations (i.e., GHG), anthropogenic aerosols (i.e., AAER), biomass burning emissions (i.e., BMB), and forcings other than GHG, AAER, and BMB (i.e., EE). The external forcings in the EE experiment include land-use changes, time-varying ozone concentrations, and natural forcings (i.e., volcanic eruptions and time-varying solar activity). The temporal evolution of the stratospheric ozone concentration over the Antarctic, anthropogenic aerosols and other forcing agents can be found in Fig. 1 of ref. 60. We also used the CMIP6 hist-noLu⁶⁴ simulations in conjunction with the corresponding historical simulations to estimate the influences of land-use changes. To additionally infer stratospheric ozone-induced changes, along with the all-forcing experiment, we analyzed model simulations conducted under the CMIP6 hist-1950HC scenario for 1950–2014, in which ozone depleting substances (chlorofluorocarbon and hydrochlorofluorocarbon) were fixed at their 1950 levels, but with other forcing agents identical to those of the all-forcing experiment⁶⁶. Given the time-invariant concentrations of ozone depleting substances in the hist-1950HC, the ensemble-mean differences with the corresponding all-forcing experiment (i.e., historical minus hist-1950HC) can be regarded as perturbations resulting from stratospheric ozone

depletion and its feedback/interactions with greenhouse gas increases, including the warming effect of ozone depleting substances as greenhouse gases^{70–73}. Due to the unavailability of SST output from the CMIP6 archive for some cases of the hist-1950HC experiment, we instead used surface skin temperature output to examine stratospheric ozone-induced SST changes for the historical minus hist-1950HC simulations, which may cause potential errors, particularly over sea ice-covered regions. Supplementary Table 1 provides information on the model simulations analyzed in this study.

EOF analysis

An empirical orthogonal function (EOF) analysis is applied to observed annual-mean SST time series in the Pacific (70°S–60°N, 120°E–60°W) in order to determine dominant modes of variability over a given period. Before conducting EOF analysis, we smoothed the time series by applying a 7-year running average to reduce interannual and shorter-time scale variability. The spatial pattern of a given EOF mode is presented by regressing SST anomalies onto the corresponding standardized principal component (PC).

Inter-ensemble EOF analysis

By conducting an additional EOF analysis across ensemble members (i.e., interensemble-wise EOF) of a given model for simulated SST trends in the Pacific, we explored the possibility that the observed tropical eastern Pacific cooling trend is linked in part to internal climate variability. As the ensemble members were integrated under the same external forcing but with different initial conditions, the resulting leading EOF mode, which represents the dominant mode of inter-ensemble variability, is mainly related to internal climate variability. Then, on the basis of the corresponding PC values, composite mean trends are computed, respectively, for the ensemble members whose PC values are at the top 10% and at the bottom 10% to examine whether the two subsets are substantially different from each other (due to internal variability).

Sensitivity of observed SST trend to analysis period

To determine whether the spatial pattern of SST trends in the Pacific might vary substantially depending on selected time periods, SST trends are computed for multiple cases, in which the time span ranges from 22 to 73 years, by changing the starting and ending years. For instance, 22-year trends can be computed over various 22-year periods such as 1950–1971, 1951–1972, ..., 2001–2022. In the case of the 73-year period, trends are computed only over the period 1950–2022. The spatial pattern correlation between the computed SST trend and the La Niña-like pattern is then determined to examine whether Pacific SST trends have persistently exhibited a La Niña-like pattern.

Test on the role of internal climate variability in the tropical eastern Pacific cooling trend

Considering well-known model biases and deficiencies^{3,4,8,10,11,35,40,46} including missing Antarctic meltwater discharge³, the observed tropical eastern Pacific cooling trend might have resulted from greenhouse gas forcing with internal climate variability playing a minor role. It is also possible that climate models may have deficiency in simulating the linkage between stratospheric ozone depletion and the tropical eastern Pacific cooling trend due to a potential limitation in model resolution to resolve the full-strength impact of stratospheric ozone depletion⁸⁷, apart from potentially underestimating the impact. To address these questions, we conducted an EOF analysis over the Pacific for 1953–2019 using the SST anomaly difference between ERSST5 and the model-simulated ensemble mean. If the model-simulated forced response is largely consistent with reality, the resultant EOF and PC are expected to exhibit a feature that is closely linked to observed low-frequency internal climate variability such as the IPO. The EOF and related atmospheric circulation anomaly patterns are also compared with those for pre-industrial control simulations in which there is no change in external forcing agents.

Statistical information

In this study, the standard least squares linear regression approach is used to compute trends and regression coefficients. Statistical significance of the computed trends and regression coefficients is assessed using a two-sided Student's *t*-test at the 95% confidence level with reduced degrees of freedom to account for autocorrelation in a given time series. In the case of model-simulated trends, the statistical significance is determined by checking whether more than 70% of the model simulations exhibit the same sign.

Data availability

The ERSST5 data set is available at <https://psl.noaa.gov/data/gridded/data.noaa.ersst.v5.html>, the ERA5 data set at <https://cds.climate.copernicus.eu>, the HadISST data set at <https://www.metoffice.gov.uk/hadobs/hadisst/data/download.html>, the CESM2 Large Ensemble output at <https://www.cesm.ucar.edu/projects/community-projects/LENS2/data-sets.html>, the CESM2 Single Forcing Large Ensemble Project output at <https://www.cesm.ucar.edu/working-groups/climate/simulations/cesm2-single-forcing-le>, the CMIP6 simulation output at <https://esgf-node.llnl.gov/projects/cmip6/>, and the low-pass filtered IPO index at <https://psl.noaa.gov/data/timeseries/IPOTPI/>.

Code availability

The code used to generate the figures in this study is freely available at <https://doi.org/10.5281/zenodo.11647501>.

Received: 9 January 2024; Accepted: 4 July 2024;

Published online: 24 July 2024

References

- Rasmusson, E. M. & Wallace, J. M. Meteorological aspects of the El Niño/Southern Oscillation. *Science* **222**, 1195–1202 (1983).
- Yeh, S.-W. et al. ENSO atmospheric teleconnections and their response to greenhouse gas forcing. *Rev. Geophys.* **56**, 185–206 (2018).
- Dong, Y., Pauling, A. G., Sadai, S. & Armour, K. C. Antarctic ice-sheet meltwater reduces transient warming and climate sensitivity through the sea-surface temperature pattern effect. *Geophys. Res. Lett.* **49**, e2022GL101249 (2022).
- Lee, S. et al. On the future zonal contrasts of equatorial Pacific climate: Perspectives from observations, simulations, and theories. *npj Clim. Atmos. Sci.* **5**, 82 (2022).
- Xiang, B., Wang, B. & Li, T. A new paradigm for the predominance of standing Central Pacific warming after the late 1990s. *Clim. Dyn.* **41**, 327–340 (2013).
- Hu, Z.-Z. et al. Weakened interannual variability in the tropical Pacific Ocean since 2000. *J. Clim.* **26**, 2601–2613 (2013).
- L'Heureux, M. L., Collins, D. C. & Hu, Z.-Z. Linear trends in sea surface temperature of the tropical Pacific Ocean and implications for the El Niño–Southern Oscillation. *Clim. Dyn.* **40**, 1223–1236 (2013).
- Luo, J.-J., Wang, G. & Dommenges, D. May common model biases reduce CMIP5's ability to simulate the recent Pacific La Niña-like cooling? *Clim. Dyn.* **50**, 1335–1351 (2018).
- Hartmann, D. L. The Antarctic ozone hole and the pattern effect on climate sensitivity. *Proc. Natl Acad. Sci. USA* **119**, e2207889119 (2022).
- Wills, R. C. J., Dong, Y., Proistosescu, C., Armour, K. C. & Battisti, D. S. Systematic climate model biases in the large-scale patterns of recent sea-surface temperature and sea-level pressure change. *Geophys. Res. Lett.* **49**, e2022GL100011 (2022).
- Latif, M. et al. Strengthening atmospheric circulation and trade winds slowed tropical Pacific surface warming. *Commun. Earth Environ.* **4**, 249 (2023).
- Hu, Z.-Z. et al. The interdecadal shift of ENSO properties in 1999/2000: A review. *J. Clim.* **33**, 4441–4462 (2020).
- Li, X., Hu, Z.-Z. & Becker, E. On the westward shift of tropical Pacific climate variability since 2000. *Clim. Dyn.* **53**, 2905–2918 (2019).
- Li, X., Hu, Z.-Z., Huang, B. & Jin, F.-F. On the interdecadal variation of the warm water volume in the tropical Pacific around 1999/2000. *J. Geophys. Res. Atmos.* **125**, e2020JD033306 (2020).
- McPhaden, M. J. A 21st century shift in the relationship between ENSO SST and warm water volume anomalies. *Geophys. Res. Lett.* **39**, L09706 (2012).
- Barnston, A. G., Tippett, M. K., L'Heureux, M. L., Li, S. & Dewitt, D. G. Skill of real-time seasonal ENSO model predictions during 2002–2011: Is our capability increasing? *Bull. Am. Meteorol. Soc.* **93**, 631–651 (2012).
- Li, X., Hu, Z.-Z., McPhaden, M. J., Zhu, C. & Liu, Y. Triple-Dip La Niñas in 1998–2001 and 2020–2023: Impact of mean state changes. *J. Geophys. Res. Atmos.* **128**, e2023JD038843 (2023).
- Clement, A. C., Seager, R., Cane, M. A. & Zebiak, S. E. An ocean dynamical thermostat. *J. Clim.* **9**, 2190–2196 (1996).
- Heede, U. K. & Fedorov, A. V. Eastern equatorial Pacific warming delayed by aerosols and thermostat response to CO₂ increase. *Nat. Clim. Change* **11**, 696–703 (2021).
- Kohyama, T., Hartmann, D. L. & Battisti, D. S. La Niña-like mean-state response to global warming and potential oceanic roles. *J. Clim.* **30**, 4207–4225 (2017).
- McGregor, S. et al. Recent Walker circulation strengthening and Pacific cooling amplified by Atlantic warming. *Nat. Clim. Change* **4**, 888–892 (2014).
- Li, X., Xie, S.-P., Gille, S. T. & Yoo, C. Atlantic-induced pan-tropical climate change over the past three decades. *Nat. Clim. Change* **6**, 275–279 (2016).
- Zhang, L. et al. Indian Ocean warming trend reduces Pacific warming response to anthropogenic greenhouse gases: An interbasin thermostat mechanism. *Geophys. Res. Lett.* **46**, 10,882–10,890 (2019).
- Cai, W. et al. Pan-tropical climate interactions. *Science* **363**, eaav4236 (2019).
- Lee, S.-K., Kim, D., Foltz, G. R. & Lopez, H. Pan-tropical response to global warming and the emergence of a La Niña-like mean state trend. *Geophys. Res. Lett.* **47**, e2019GL086497 (2020).
- Takahashi, C. & Watanabe, M. Pacific trade winds accelerated by aerosol forcing over the past two decades. *Nat. Clim. Change* **6**, 768–772 (2016).
- Qin, M., Dai, A. & Hua, W. Aerosol-forced multidecadal variations across all ocean basins in models and observations since 1920. *Sci. Adv.* **6**, eaab0425 (2020).
- Dittus, A. J., Hawkins, E., Robson, J. I., Smith, D. M. & Wilcox, L. J. Drivers of recent North Pacific decadal variability: The role of aerosol forcing. *Earth's Future* **9**, e2021EF002249 (2021).
- Hwang, Y.-T., Xie, S.-P., Chen, P.-J., Tseng, H.-Y. & Deser, C. Contribution of anthropogenic aerosols to persist La Niña-like conditions in the early 21st century. *Proc. Natl Acad. Sci. USA* **121**, e2315124121 (2024).
- Kim, H., Kang, S. M., Kay, J. E. & Xie, S.-P. Subtropical clouds key to Southern Ocean teleconnections to the tropical Pacific. *Proc. Natl Acad. Sci. USA* **119**, e2200514119 (2022).
- Kang, S. M., Shin, Y., Kim, H., Xie, S.-P. & Hu, S. Disentangling the mechanisms of equatorial Pacific climate change. *Sci. Adv.* **9**, eadf5059 (2023).
- Dong, L. & Zhou, T. The formation of the recent cooling in the eastern tropical Pacific Ocean and the associated climate impacts: A competition of global warming, IPO, and AMO. *J. Geophys. Res. Atmos.* **119**, 11,272–11,287 (2014).
- Meehl, G. A., Hu, A., Arblaster, J. M., Fasullo, J. & Trenberth, K. E. Externally forced and internally generated decadal climate variability associated with the Interdecadal Pacific Oscillation. *J. Clim.* **26**, 7298–7310 (2013).

34. Bordbar, M. H., Martin, T., Latif, M. & Park, W. Role of internal variability in recent decadal to multidecadal tropical Pacific climate changes. *Geophys. Res. Lett.* **44**, 4246–4255 (2017).
35. Seager, R. et al. Strengthening tropical Pacific zonal sea surface temperature gradient consistent with rising greenhouse gases. *Nat. Clim. Change* **9**, 517–522 (2019).
36. Olonscheck, D., Rugenstein, M. & Marotzke, J. Broad consistency between observed and simulated trends in sea surface temperature patterns. *Geophys. Res. Lett.* **47**, e2019GL086773 (2020).
37. Watanabe, M., Dufresne, J.-L., Kosaka, Y., Mauritzen, T. & Tatebe, H. Enhanced warming constrained by past trends in equatorial Pacific sea surface temperature gradient. *Nat. Clim. Change* **11**, 33–37 (2021).
38. Deser, C., Phillips, A. S. & Alexander, M. A. Twentieth century tropical sea surface temperature trends revisited. *Geophys. Res. Lett.* **37**, L10701 (2010).
39. Solomon, A. & Newman, M. Reconciling disparate twentieth-century Indo-Pacific ocean temperature trends in the instrumental record. *Nat. Clim. Change* **2**, 691–699 (2012).
40. Seager, R., Henderson, N. & Cane, M. Persistent discrepancies between observed and modeled trends in the tropical Pacific Ocean. *J. Clim.* **35**, 4571–4584 (2022).
41. Banerjee, A., Fyfe, J. C., Polvani, L. M., Waugh, D. & Chang, K.-L. A pause in Southern Hemisphere circulation trends due to the Montreal Protocol. *Nature* **579**, 544–548 (2020).
42. Polvani, L. M. et al. Interannual SAM modulation of Antarctic sea ice extent does not account for its long-term trends, pointing to a limited role for ozone depletion. *Geophys. Res. Lett.* **48**, e2021GL094871 (2021).
43. Kang, S. M. et al. Global impacts of recent Southern Ocean cooling. *Proc. Natl Acad. Sci. USA* **120**, e2300881120 (2023).
44. Kravtsov, S., Grimm, C. & Gu, S. Global-scale multidecadal variability missing in state-of-the-art climate models. *npj Clim. Atmos. Sci.* **1**, 34 (2018).
45. Song, F. & Zhang, G. J. Effects of southeastern Pacific sea surface temperature on the double-ITCZ bias in NCAR CESM1. *J. Clim.* **29**, 7417–7433 (2016).
46. Heede, U. K. & Fedorov, A. V. Colder eastern equatorial Pacific and stronger Walker circulation in the early 21st century: Separating the forced response to global warming from natural variability. *Geophys. Res. Lett.* **50**, e2022GL101020 (2023).
47. Okumura, Y. M. Origins of tropical Pacific decadal variability: Role of stochastic atmospheric forcing from the South Pacific. *J. Clim.* **26**, 9791–9796 (2013).
48. Polvani, L. M. & Smith, K. L. Can natural variability explain observed Antarctic sea ice trends? New modeling evidence from CMIP5. *Geophys. Res. Lett.* **40**, 3195–3199 (2013).
49. Fan, T., Deser, C. & Schneider, D. P. Recent Antarctic sea ice trends in the context of Southern Ocean surface climate variations since 1950. *Geophys. Res. Lett.* **41**, 2419–2426 (2014).
50. Chung, E.-S. et al. Reconciling opposing Walker circulation trends in observations and model projections. *Nat. Clim. Change* **9**, 405–412 (2019).
51. Chung, E.-S. et al. Antarctic sea-ice expansion and Southern Ocean cooling linked to tropical variability. *Nat. Clim. Change* **12**, 461–468 (2022).
52. Henley, B. J. et al. A Tripole Index for the Interdecadal Pacific Oscillation. *Clim. Dyn.* **45**, 3077–3090 (2015).
53. Li, X. et al. Tropical teleconnection impacts on Antarctic climate changes. *Nat. Rev. Earth Environ.* **2**, 680–698 (2021).
54. Schneider, D. P., Deser, C. & Fan, T. Comparing the impacts of tropical SST variability and polar stratospheric ozone loss on the Southern Ocean westerly winds. *J. Clim.* **28**, 9350–9372 (2015).
55. Meehl, G. A., Arblaster, J. M., Bitz, C. M., Chung, C. T. Y. & Teng, H. Antarctic sea-ice expansion between 2000 and 2014 driven by tropical Pacific decadal climate variability. *Nat. Geosci.* **9**, 590–595 (2016).
56. Purich, A. et al. Tropical Pacific SST drivers of recent Antarctic sea ice trends. *J. Clim.* **29**, 8931–8948 (2016).
57. Jun, S.-Y. et al. The internal origin of the west-east asymmetry of Antarctic climate change. *Sci. Adv.* **6**, eaaz1490 (2020).
58. Lee, S.-K. et al. Human-induced changes in the global meridional overturning circulation are emerging from the Southern Ocean. *Commun. Earth Environ.* **4**, 69 (2023).
59. Rodgers, K. B. et al. Ubiquity of human-induced changes in climate variability. *Earth. Syst. Dynam.* **12**, 1393–1411 (2021).
60. Simpson, I. R. et al. The CESM2 Single-Forcing Large Ensemble and comparison to CESM1: Implications for experimental design. *J. Clim.* **36**, 5687–5711 (2023).
61. Gillett, N. P. et al. The Detection and Attribution Model Intercomparison Project (DAMIP v1.0) contribution to CMIP6. *Geosci. Model Dev.* **9**, 3685–3697 (2016).
62. Thompson, D. W. J. et al. Signatures of the Antarctic ozone hole in Southern Hemisphere surface climate change. *Nat. Geosci.* **4**, 741–749 (2011).
63. Kushner, P. J., Held, I. M. & Delworth, T. L. Southern Hemisphere atmospheric circulation response to global warming. *J. Clim.* **14**, 2238–2249 (2001).
64. Lawrence, D. M. et al. The Land Use Model Intercomparison Project (LUMIP) contribution to CMIP6: rationale and experimental design. *Geosci. Model Dev.* **9**, 2973–2998 (2016).
65. Skeie, R. B. et al. Historical total ozone radiative forcing derived from CMIP6 simulations. *npj. Clim. Atmos. Sci.* **3**, 32 (2020).
66. Collins, W. J. et al. AerChemMIP: quantifying the effects of chemistry and aerosols in CMIP6. *Geosci. Model Dev.* **10**, 585–607 (2017).
67. Mechoso, C. R. et al. Can reducing the incoming energy flux over the Southern Ocean in a CGCM improve its simulation of tropical climate? *Geophys. Res. Lett.* **43**, 11057–11063 (2016).
68. Polvani, L. M., Waugh, D. W., Correa, G. J. P. & Son, S.-W. Stratospheric ozone depletion: The main driver of twentieth-century atmospheric circulation changes in the Southern Hemisphere. *J. Clim.* **24**, 795–812 (2011).
69. Kang, S. M., Polvani, L. M., Fyfe, J. C. & Sigmond, M. Impact of polar ozone depletion on subtropical precipitation. *Science* **332**, 951–954 (2011).
70. Smith, D. M. et al. Role of volcanic and anthropogenic aerosols in the recent global surface warming slowdown. *Nat. Clim. Change* **6**, 936–940 (2016).
71. Polvani, L. M. & Bellomo, K. The key role of ozone-depleting substances in weakening the Walker circulation in the second half of the twentieth century. *J. Clim.* **32**, 1411–1418 (2019).
72. Polvani, L. M., Previdi, M., England, M. R., Chiodo, G. & Smith, K. L. Substantial twentieth-century Arctic warming caused by ozone-depleting substances. *Nat. Clim. Change* **10**, 130–133 (2020).
73. Sigmond, M. et al. Large contribution of ozone-depleting substances to global and Arctic warming in the late 20th century. *Geophys. Res. Lett.* **50**, e2022GL100563 (2023).
74. Vecchi, G. A. et al. Weakening of tropical Pacific atmospheric circulation due to anthropogenic forcing. *Nature* **441**, 73–76 (2006).
75. Jha, B., Hu, Z.-Z. & Kumar, A. SST and ENSO variability and change simulated in historical experiments of CMIP5 models. *Clim. Dyn.* **42**, 2113–2124 (2014).
76. Dong, Y., Polvani, L. M. & Bonan, D. B. Recent multi-decadal Southern Ocean surface cooling unlikely caused by Southern Annular Mode trends. *Geophys. Res. Lett.* **50**, e2023GL106142 (2023).
77. Sen Gupta, A. & England, M. H. Coupled ocean-atmosphere feedback in the Southern Annular Mode. *J. Clim.* **20**, 3677–3692 (2007).
78. Deser, C. et al. Isolating the evolving contributions of anthropogenic aerosols and greenhouse gases: A new CESM1 Large Ensemble Community resource. *J. Clim.* **33**, 7835–7858 (2020).

79. Wang, P. et al. Aerosols overtake greenhouse gases causing a warmer climate and more weather extremes toward carbon neutrality. *Nat. Commun.* **14**, 7257 (2023).
80. Wang, B. et al. Toward predicting changes in the land monsoon rainfall a decade in advance. *J. Clim.* **31**, 2699–2714 (2018).
81. Cai, W. et al. Changing El Niño–Southern Oscillation in a warming climate. *Nat. Rev. Earth Environ.* **2**, 628–644 (2021).
82. Huang, B. et al. Extended Reconstructed Sea Surface Temperature, Version 5 (ERSSTv5): Upgrades, validations, and intercomparisons. *J. Clim.* **30**, 8179–8205 (2017).
83. Hersbach, H. et al. The ERA5 global reanalysis. *Q. J. R. Meteorol. Soc.* **146**, 1999–2049 (2020).
84. Rayner, N. A. et al. Global analyses of sea surface temperature, sea ice, and night marine air temperature since the late nineteenth century. *J. Geophys. Res.* **108**, 4407 (2003).
85. Chemke, R. & Yuval, J. Human-induced weakening of the Northern Hemisphere tropical circulation. *Nature* **617**, 529–532 (2023).
86. Eyring, V. et al. Overview of the Coupled Model Intercomparison Project Phase 6 (CMIP6) experimental design and organization. *Geosci. Model Dev.* **9**, 1937–1958 (2016).
87. Marsh, D. R. et al. Climate change from 1850 to 2005 simulated in CESM1(WACCM). *J. Clim.* **26**, 7372–7391 (2013).

Acknowledgements

We acknowledge Prof. Sukyoung Lee for helpful discussions and comments. We are grateful to the National Oceanic and Atmospheric Administration Physical Sciences Laboratory, the European Centre for Medium Range Weather Forecasts, British Antarctic Survey, the Met Office Hadley Centre, and modeling centers for providing their respective data sets. E.-S.C. was supported by Korea Polar Research Institute (KOPRI) grants funded by the Ministry of Oceans and Fisheries (KOPRI PE23340 and PE24030). S.-J.K., S.-Y.J., and J.-H.K. were supported by KOPRI grant PE24030. K.-J.H. was supported by the Institute for Basic Science (IBS) under IBS-R028-D1. Y.S.K. was supported by Korea Institute of Marine Science & Technology Promotion (KIMST) funded by the Ministry of Oceans and Fisheries (RS-2022-KS221667).

Author contributions

E.-S.C., S.-J.K., and S.-K.L. designed the study. E.-S.C. performed the analysis and produced figures. S.-J.K., S.-K.L., K.-J.H., S.-W.Y., Y.S.K., S.-Y.J., J.-H.K., and D.K. provided feedback on the analyses, interpretation of the results, and the figures. All authors contributed to the writing of the manuscript and improvement of the manuscript.

Competing interests

The authors declare no competing interests.

Additional information

Supplementary information The online version contains supplementary material available at <https://doi.org/10.1038/s41612-024-00713-2>.

Correspondence and requests for materials should be addressed to Seong-Joong Kim.

Reprints and permissions information is available at <http://www.nature.com/reprints>

Publisher's note Springer Nature remains neutral with regard to jurisdictional claims in published maps and institutional affiliations.

Open Access This article is licensed under a Creative Commons Attribution 4.0 International License, which permits use, sharing, adaptation, distribution and reproduction in any medium or format, as long as you give appropriate credit to the original author(s) and the source, provide a link to the Creative Commons licence, and indicate if changes were made. The images or other third party material in this article are included in the article's Creative Commons licence, unless indicated otherwise in a credit line to the material. If material is not included in the article's Creative Commons licence and your intended use is not permitted by statutory regulation or exceeds the permitted use, you will need to obtain permission directly from the copyright holder. To view a copy of this licence, visit <http://creativecommons.org/licenses/by/4.0/>.

© The Author(s) 2024